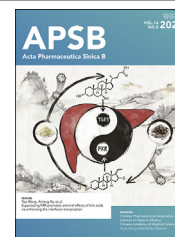




Chinese Pharmaceutical Association
Institute of Materia Medica, Chinese Academy of Medical Sciences

Acta Pharmaceutica Sinica B

www.elsevier.com/locate/apsb
www.sciencedirect.com



ORIGINAL ARTICLE

Discovery of TK-642 as a highly potent, selective, orally bioavailable pyrazolopyrazine-based allosteric SHP2 inhibitor



Kai Tang^{a,†}, Shu Wang^{a,†}, Siqi Feng^{a,†}, Xinyu Yang^{a,†}, Yueyang Guo^a,
Xiangli Ren^a, Linyue Bai^a, Bin Yu^{b,c,d,*}, Hong-Min Liu^{a,*},
Yihui Song^{a,*}

^aSchool of Pharmaceutical Sciences & Key Laboratory of Advanced Drug Preparation Technologies, Ministry of Education, Zhengzhou University, Zhengzhou 450001, China

^bCollege of Chemistry, Pingyuan Laboratory, State Key Laboratory of Antiviral Drugs, Zhengzhou University, Zhengzhou 450001, China

^cTianjian Laboratory of Advanced Biomedical Sciences, Institute of Advanced Biomedical Sciences, Zhengzhou University, Zhengzhou 450000, China

^dState Key Laboratory of Pharmaceutical Biotechnology, Nanjing University, Nanjing 210023, China

Received 13 December 2023; received in revised form 20 February 2024; accepted 14 March 2024

KEY WORDS

Protein tyrosine phosphatase;
Pyrazolopyrazine;
SHP2 inhibitor;
Esophageal cancer

Abstract Src homology-2-containing protein tyrosine phosphatase 2 (SHP2) is a promising therapeutic target for cancer therapy. In this work, we presented the structure-guided design of 5,6-fused bicyclic allosteric SHP2 inhibitors, leading to the identification of pyrazolopyrazine-based TK-642 as a highly potent, selective, orally bioavailable allosteric SHP2 inhibitor (SHP2^{WT} IC₅₀ = 2.7 nmol/L) with favorable pharmacokinetic profiles ($F = 42.5\%$; $t_{1/2} = 2.47$ h). Both dual inhibition biochemical assay and docking analysis indicated that TK-642 likely bound to the “tunnel” allosteric site of SHP2. TK-642 could effectively suppress cell proliferation (KYSE-520 cells IC₅₀ = 5.73 μmol/L) and induce apoptosis in esophageal cancer cells by targeting the SHP2-mediated AKT and ERK signaling pathways. Additionally, oral administration of TK-642 also demonstrated effective anti-tumor effects in the KYSE-520 xenograft mouse model, with a T/C value of 83.69%. Collectively, TK-642 may warrant further investigation as a promising lead compound for the treatment of esophageal cancer.

*Corresponding authors.

E-mail addresses: zzuyubin@hotmail.com (Bin Yu), liuhm@zzu.edu.cn (Hong-Min Liu), songyihui@zzu.edu.cn (Yihui Song).

[†]These authors made equal contributions to this work.

Peer review under the responsibility of Chinese Pharmaceutical Association and Institute of Materia Medica, Chinese Academy of Medical Sciences.

<https://doi.org/10.1016/j.apsb.2024.03.028>

2211-3835 © 2024 The Authors. Published by Elsevier B.V. on behalf of Chinese Pharmaceutical Association and Institute of Materia Medica, Chinese Academy of Medical Sciences. This is an open access article under the CC BY-NC-ND license (<http://creativecommons.org/licenses/by-nc-nd/4.0/>).

1. Introduction

Src homology-2-containing protein tyrosine phosphatase 2 (SHP2) is a non-receptor protein tyrosine phosphatase (PTP) encoded by the proto-oncogene *PTPN11*^{1–3}. SHP2 protein comprises 593 amino acids and includes two SH2 domains (N-SH2 and C-SH2), a well-conserved PTP domain, and a C-terminal tail with two phosphorylation sites (Tyr542 and Tyr580)⁴. Under normal physiological conditions, SHP2's interdomain interactions prevent substrate access to its active site, thereby maintaining SHP2 in an auto-inhibited inactive conformation. Nevertheless, mutations within the SH2/PTP interdomain can disrupt these interactions, ultimately leading to the interruption of auto-inhibited conformation^{5–7}. SHP2 hyperactivation, driven by germline or somatic mutations in *PTPN11*, is linked to a range of disorders including Noonan syndrome (NS), juvenile myelomonocytic leukemia (JMML), myelodysplastic syndrome (MDS), B-cell acute lymphoblastic leukemia (B-ALL), acute myeloid leukemia (AML), as well as various solid tumors (e.g., esophageal cancer, hepatocellular carcinoma, melanoma, and colon cancer)^{8–11}. Serving as a central hub in numerous signaling pathways encompassing RAS-RAF-MEK-ERK, PI3K-AKT, JAK-STAT, and PD-1/PD-L1, SHP2 plays dual roles in both the downstream effects of oncogenic drivers and cancer immune evasion^{12,13}. This underscores its potential as a promising therapeutic target for the treatment of various diseases^{14–16}.

Initially, efforts in SHP2-targeted drug discovery were primarily centered on PTP inhibitors targeting the catalytic PTP domain of SHP2 over several decades^{17–23}. However, the clinical progress of these inhibitors encountered various challenges, including limited permeability, inadequate oral bioavailability, and poor selectivity. These issues were stemmed from the inherently high polar and positively charged properties of the SHP2 catalytic pocket^{6,24,25}. It wasn't until year 2016 that substantial efforts were devoted to the development of allosteric SHP2 inhibitors, which inhibited the dephosphorylation activity of SHP2 by locking SHP2 in its auto-inhibited inactive conformation (Fig. 1A)^{25–34}. To date, fourteen SHP2 allosteric inhibitors, including TNO155, JAB-3068, JAB-3312, RMC-4630, BR-790, BBP-398, BPI-442096, ERAS-601, ICP-189, RLY-1971, SH-3809, PF-07284892, ET-0038 and HBI-2376, have advanced into clinical trials for cancer therapy^{11,35–39}. Additionally, there have been reports of several proteolysis-targeting chimera (PROTAC)-based degraders and dual inhibitors targeting SHP2, offering potential treatment options for various types of cancer^{40–45}.

Our group has also unveiled a novel set of allosteric SHP2 inhibitors with great potential as hit compounds for extensive refinement (Fig. 1B)^{46–48}. The cyclization strategy, a well-established technique in medicinal chemistry, has a demonstrated history of success in the filed of drug discovery. This approach holds promise of markedly enhancing potency and selectivity, improving pharmacodynamic and kinetic properties, and infusing novel structural elements³⁴. In our present work, we

reported structure–activity relationship (SARs) studies of a new series of 5,6-fused bicyclic allosteric SHP2 inhibitors. This effort led to the identification of TK-642, a highly potent, selective, orally efficacious allosteric SHP2 inhibitor with favorable pharmacokinetic profiles (**13i**: SHP2^{WT} IC₅₀ = 2.7 ± 0.1 nmol/L; SHP2^{WT} ΔT_m = 8.83 ± 0.11 °C; F = 42.5 ± 3.4%; t_{1/2} = 2.47 h). Through inhibiting the phosphatase activity of SHP2 and subsequently suppressing SHP2-mediated AKT and ERK signaling pathways, TK-642 treatment demonstrated notable anti-tumor efficacy against esophageal cancer both *in vivo* and *in vitro* (KYSE-520 cells IC₅₀ = 5.73 ± 0.34 μmol/L; tumor growth inhibition = 83.69 ± 10.44%).

2. Results and discussion

2.1. Design strategy

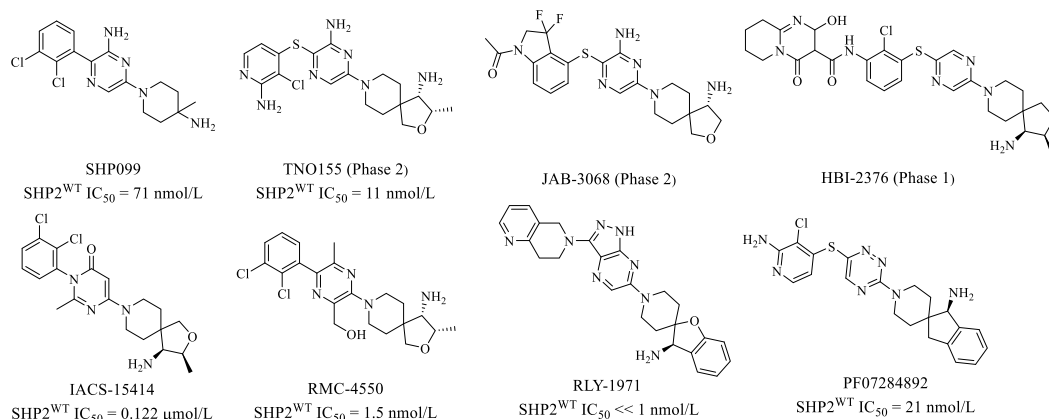
In previous studies, our research group uncovered several SHP2 inhibitors from our diverse in-house compound library^{46,48}. Among these, TK-145 emerged as a promising hit compound with an IC₅₀ value of 0.258 μmol/L against SHP2^{WT}. Docking analysis of the SHP2/TK-145 complex structure revealed several crucial interactions, as illustrated in Fig. 2A. Specifically, a hydrogen bond interaction was observed between the 4-amine of pyrimidine ring and the backbone carbonyl of E250. Moreover, the basic amine group also formed another hydrogen bond with F113. The 2,3-dichloropenyl motif, extending into a hydrophobic pocket formed by residues L254, Q257 and Q495, mediated a weak cation–π interaction with R111 (3.9 Å), which potentially offered opportunities for further optimization.

Based on the above information, we intended to explore the cyclization strategy to construct a conformationally restricted bicyclic skeleton by merging the 4-amine in the pyrimidine ring of TK-145 and the adjacent 5-carbon. Finally, a novel pyrazolopyrimidine core of compound **6a** was developed. Compound **6a** not only maintained the H-bonding of central aminopyrimidine but also potentially made the aryl motif more favorable for filling the hydrophobic cleft to mediate the cation–π interaction with R111 (Fig. 2B). Biochemical results suggested that compound **6a** showed slightly decreased inhibitory activity against SHP2^{WT} (SHP2^{WT} IC₅₀ = 1.305 μmol/L), indicating a weakened interaction between cyclized derivative **6a** and SHP2 protein for TK-145. Nevertheless, the compound still exhibited certain inhibitory activity, which might indicate the feasibility of the conformationally restricted bicyclic strategy. Subsequently, we synthesized a series of fused bicyclic SHP2 inhibitors to explore the SARs on the aromatic group, amine fragment and central bicyclic core, respectively.

2.2. Structure–activity relationship studies (SARs)

Considering the significance of aminopiperidine moiety in the potency of TK-145, compounds **6a–6k** were initially synthesized and

A. Representative allosteric SHP2 inhibitors in the literatures



B. Allosteric SHP2 inhibitors reported in our group

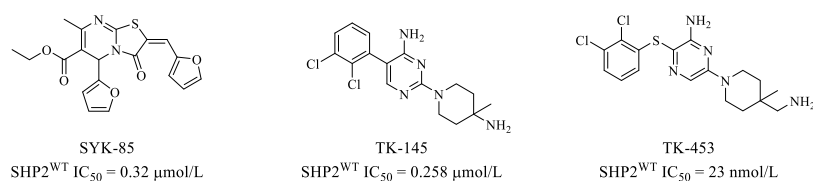


Figure 1 (A) Representative allosteric SHP2 inhibitors reported in the literatures. (B) Allosteric SHP2 inhibitors reported by our group.

evaluated for their inhibitory activities against SHP2 following our previously reported cross-validation screening procedure. The IC₅₀ values of allosteric inhibitors against SHP2^{WT} have been shown positively correlation with the ΔT_m values⁴⁶. Direct cyclization of TK-145 resulted in the generation of compound **6a**, which exhibited a moderate level of potency (SHP2^{WT} IC₅₀ = 1.305 ± 0.132 μmol/L,

SHP2^{WT} ΔT_m = 4.11 ± 0.18 °C). This observation suggested that cyclization between the 5-position and the NH₂ at the 4-position of the pyrimidine ring could provide new chemical space without significantly compromising inhibitory activity. Encouragingly, we subsequently investigated the SARs of substituents on the terminal aminopiperidine group as shown in Table 1. Eliminating the methyl

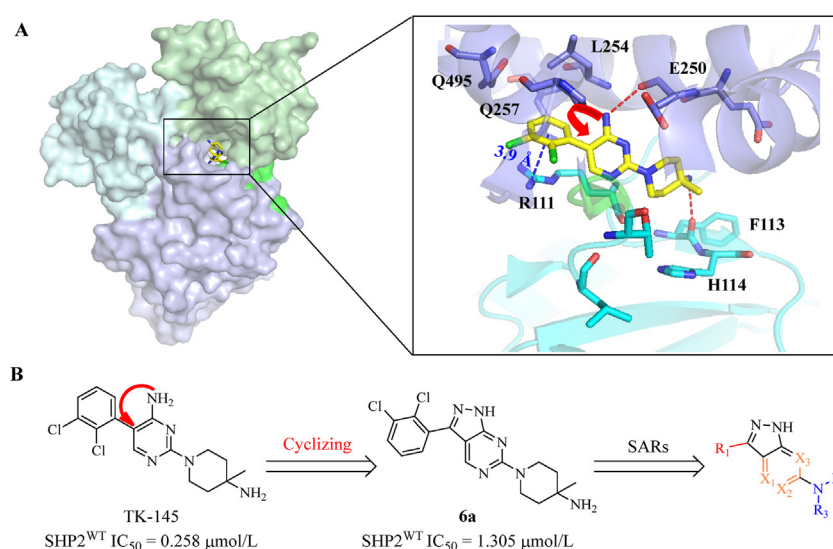
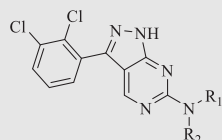


Figure 2 (A) The proposed binding mode of TK-145 with SHP2 (PDB code: 5EHR). The N-SH2 domain of SHP2 is colored in palecyan, the C-SH2 domain is colored in palegreen and the PTP domain is colored in lightblue. TK-145 is displayed in yellow stick representation. The hydrogen bond interactions between TK-145 and SHP2 are indicated by red dash lines and the cation- π interaction is indicated by blue dash lines. (B) Structure-based design of novel bicyclic SHP2 inhibitors using the cyclization strategy.

Table 1 Inhibitory effects of compounds **6a–6k** against SHP2^a.Compounds **6a–6k**

Compd.	NR ₁ R ₂	SHP2 ^{WT} IC ₅₀ (μmol/L)	SHP2 ^{WT} ΔT _m (°C)
SHP099	—	0.071 ± 0.001	4.370 ± 0.180
6a		1.305 ± 0.132	4.110 ± 0.180
6b		1.521 ± 0.140	3.110 ± 0.050
6c		5.046 ± 0.137	1.770 ± 0.050
6d		>10	N.D. ^b
6e		>10	N.D.
6f		>10	N.D.
6g		>10	N.D.
6h		4.219 ± 0.143	1.970 ± 0.080
6i		2.852 ± 0.185	2.220 ± 0.060
6j		2.168 ± 0.316	3.370 ± 0.270
6k		1.724 ± 0.381	1.160 ± 0.090

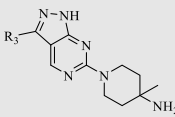
^aAll experiments were independently performed at least three times, the data are represented as the mean values.

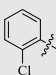
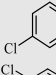
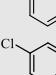
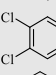
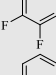
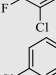
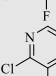
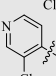
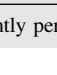
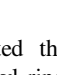
^bN.D. means not determined.

substitution in **6a** showed comparable inhibitory activity against SHP2^{WT} (**6b**: SHP2^{WT} IC₅₀ = 1.521 ± 0.140 μmol/L, SHP2^{WT} ΔT_m = 3.110 ± 0.050 °C), whereas extending terminal amino side chain resulted in a notable reduction in both inhibitory activities and the change in melting temperature (**6c**: SHP2^{WT} IC₅₀ = 5.046 ± 0.137 μmol/L, SHP2^{WT} ΔT_m = 1.770 ± 0.050 °C; **6d**: SHP2^{WT} IC₅₀ > 10 μmol/L). Similarly, substituting the amino group with dimethylamino (**6e**) or a hydroxyl group (**6f**), or replacing the aminopiperidine ring with an aminopyrrolidine ring (**6g**), also led to significantly decreased inhibitory activities against SHP2^{WT} (IC₅₀ > 10 μmol/L). This demonstrated that the presence of a six-membered ring with an amino group at the 4-position was more favorable for the potency of compounds. This rule was further confirmed by the observation that both the piperazine analog **6h** (SHP2^{WT} IC₅₀ = 4.219 ± 0.143 μmol/L, SHP2^{WT} ΔT_m = 1.970 ± 0.080 °C) and the methylpiperazine analog **6i** (SHP2^{WT} IC₅₀ = 2.852 ± 0.185 μmol/L, SHP2^{WT} ΔT_m = 2.220 ± 0.060 °C) exhibited slightly lower potency against SHP2^{WT} than **6b**. Interestingly, elongating the amino substituent on the piperidine ring with a methylene group resulted in compound **6j** (SHP2^{WT} IC₅₀ = 2.168 ± 0.316 μmol/L, SHP2^{WT}

ΔT_m = 3.370 ± 0.270 °C) with decreased potency. Furthermore, its cyclized counterpart, compound **6k**, also exhibited appreciable potency against SHP2^{WT} with an IC₅₀ value of 1.724 ± 0.381 μmol/L and a ΔT_m value of 1.160 ± 0.090 °C.

In a parallel study, SARs concerning the aromatic region of the cyclized compound **6a** were also explored. A series of aryl and heteroaryl derivatives **8a–8s** were synthesized and evaluated for their inhibitory activities against SHP2 (Table 2). Comparative analysis of the inhibitory activity of compounds **8a–8e** suggested that the enhanced potency (**8c**: SHP2^{WT} IC₅₀ = 0.228 ± 0.006 μmol/L, SHP2^{WT} ΔT_m = 2.560 ± 0.360 °C) primarily stemmed from the establishment of *van der Waals* contact facilitated by the chloro substituents at different positions, rather than variations in the dihedral angle of the biaryl axis. Substituting the chloro moiety with a fluorine atom at different positions (compounds **8f–8h**) did not result in a significant decreased potency, whereas replacing the dichlorophenyl ring of **6a** with the corresponding 2,3-dichloropyridine ring (**8i**) or 3-chloropyridine ring (**8j**) led to a modest increase in inhibitory activity (**8i**: SHP2^{WT} IC₅₀ = 0.696 ± 0.077 μmol/L, SHP2^{WT} ΔT_m = 3.260 ± 0.060 °C; **8j**: SHP2^{WT} IC₅₀ = 0.639 ± 0.066 μmol/L, SHP2^{WT} ΔT_m = 2.030 ± 0.020 °C).

Table 2 Inhibitory effects of compounds **8a–8j** against SHP2^a.


Compd.	R ₃	SHP2 ^{WT} IC ₅₀ (μmol/L)	SHP2 ^{WT} Δ <i>T</i> _m (°C)
SHP099	—	0.071 ± 0.001	4.370 ± 0.180
8a		1.041 ± 0.025	2.940 ± 0.030
8b		1.176 ± 0.135	2.830 ± 0.030
8c		0.228 ± 0.006	2.560 ± 0.360
8d		3.268 ± 0.301	2.650 ± 0.020
8e		2.013 ± 0.282	2.510 ± 0.050
8f		1.439 ± 0.087	2.690 ± 0.050
8g		0.965 ± 0.005	2.950 ± 0.030
8h		1.495 ± 0.082	3.060 ± 0.060
8i		0.696 ± 0.077	3.260 ± 0.060
8j		0.639 ± 0.066	2.030 ± 0.020

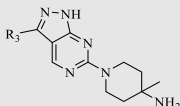
^aAll experiments were independently performed at least three times, the data are represented as the mean values.

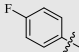
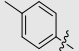
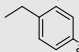
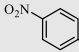
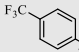
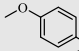
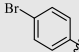
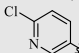
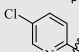
The preceding findings indicated that suitable substituents involving the chloro atom and phenyl ring may be well-tolerated. Consequently, we proceeded to investigate the impact of substituents at the 4-position of the benzene ring on the inhibitory activity against SHP2 (Table 3). Incorporation of electron-withdrawing or electron-donating substitutions, such as fluorine (**8k**), methyl (**8l**), ethyl (**8m**), nitro (**8n**), trifluoromethyl (**8o**), or methoxy (**8p**), still retained their inhibitory activities against SHP2, albeit with a reduction in potency ranging from 4- to 9-fold. Notably, the *para*-bromine analog **8q** (SHP2^{WT} IC₅₀ = 0.268 ± 0.007 μmol/L, SHP2^{WT} Δ*T*_m = 2.490 ± 0.040 °C) displayed comparable potency. Replacing the optimal 4-chlorobenzene group with a 2-chloropyridine group (**8r**: SHP2^{WT} IC₅₀ = 0.994 ± 0.043 μmol/L, SHP2^{WT} Δ*T*_m = 2.540 ± 0.010 °C) led to a 4-fold reduction in inhibitory activity, whereas the 3-chloropyridine group (**8s**: SHP2^{WT} IC₅₀ > 10 μmol/L) was unfavorable.

With the preferred 4-chlorobenzene group of compound **8c** in hand, we decided to further explore the SARs of the central bicyclic core (Table 4). Unexpectedly, compounds **13a** and **13b** showed no inhibitory activities against SHP2 with IC₅₀ values > 10 μmol/L, despite retaining the key functional groups essential for critical ligand–protein interactions. Conversely, another analog **13c** showed moderately decreased potency (SHP2^{WT} IC₅₀ = 1.145 ± 0.024 μmol/L, SHP2^{WT}

Δ*T*_m = 2.870 ± 0.080 °C), underscoring the significance of the pyrazole group in enzyme activity. In light of these results, we purposefully synthesized the target compound **13d** via preserving the pyrazole group while replacing the pyrimidine motif with a pyrazine group. Encouragingly, **13d** exhibited enhanced potency against SHP2^{WT} with an IC₅₀ value of 0.189 ± 0.004 μmol/L and a Δ*T*_m value of 2.260 ± 0.330 °C.

Inspired by the promising attributes of the 1*H*-pyrazolo [3,4-*b*]pyridine system within **13d** and the thioether linker explored in our previous study⁴⁸, we integrated the thioether linker into the biaryl core of **13d** and then yielded compound **13e** (Table 5). Rewardingly, **13e** displayed enhanced biochemical activity against SHP2^{WT} (IC₅₀ = 0.114 ± 0.001 μmol/L) and improved change in melting temperature (Δ*T*_m = 4.68 ± 0.03 °C). Additionally, regarding the correlation between the 3-chloropyridine motif and low hERG affinity, we proceeded to replace the 4-chlorobenzene ring with other favorable groups to mitigate the potential cardiac toxicity of compounds³¹. This led to the synthesis of compounds **13f–13g**, which showed a substantial increase in enzymatic activity with IC₅₀ values ranging from 0.011 to 0.023 μmol/L. This observation suggested that the molecular flexibility of these compounds may also play a pivotal role in enhancing inhibitory activity.

Table 3 Inhibitory effects of compounds **8k–8s** against SHP2^a.


Compd.	R ₃	SHP2 ^{WT} IC ₅₀ (μmol/L)	SHP2 ^{WT} Δ <i>T</i> _m (°C)
8k		1.066 ± 0.076	2.410 ± 0.040
8l		0.789 ± 0.064	2.190 ± 0.020
8m		0.904 ± 0.047	1.910 ± 0.010
8n		1.838 ± 0.202	1.880 ± 0.040
8o		1.427 ± 0.087	2.160 ± 0.090
8p		1.155 ± 0.044	1.630 ± 0.030
8q		0.268 ± 0.007	2.490 ± 0.040
8r		0.994 ± 0.043	2.540 ± 0.010
8s		>10	N.D. ^b

^aAll experiments were independently performed at least three times, the data are represented as the mean values.

^bN.D. means not determined.

Finally, considering the potential benefits of extending the amino substituent on the piperidine ring with a methylene group observed in our previous study, we purposely synthesized the corresponding compound **13i** (Table 6), also known as TK-642. As anticipated, **13i** exhibited outstanding potency against SHP2 (SHP2^{WT} IC₅₀ = 0.0027 ± 0.0001 μmol/L, SHP2^{WT} Δ*T*_m = 8.83 ± 0.11 °C). However, introducing conformational constraint by incorporating the terminal amine into a more rigid spirocyclic ring system (**13j**: SHP2^{WT} IC₅₀ = 0.0549 ± 0.002 μmol/L, SHP2^{WT} Δ*T*_m = 5.080 ± 0.050 °C) led to a significant reduction in enzymatic activity.

2.3. TK-642 is a highly potent and selective allosteric SHP2 inhibitor

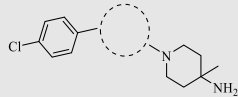
The most potent compound TK-642 (SHP2^{WT} IC₅₀ = 0.0027 ± 0.0001 μmol/L) was selected as a lead compound for subsequent evaluation, with SHP099 (SHP2^{WT} IC₅₀ = 0.0071 ± 0.0012 μmol/L) as a positive control. The assessment of SHP2^{PTP} dephosphorylation activity revealed that TK-642 exhibited negligible inhibitory activity against SHP2^{PTP} (1.5% inhibition at 10 μmol/L), underscoring its allosteric regulatory effect. Moreover, TK-642 treatment induced a 2-fold greater change in melting temperature with a Δ*T*_m value of 8.83 ± 0.105 °C than that of SHP099 (Δ*T*_m = 4.37 ± 0.18 °C). Consequently, we postulated that TK-642 exerted its allosteric inhibitory mechanism on SHP2 by impeding the dissociation of the N-SH2 domain from the PTP domain during thermal denaturation. Furthermore, enzymatic kinetics analysis revealed that the dissociation constant of TK-642 (*K*_i = 1.53 ± 0.02 nmol/L) for SHP2 was also notably enhanced,

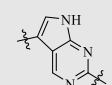
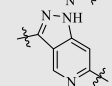
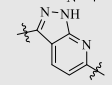
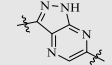
exhibiting a 45-fold improvement over SHP099 (*K*_i = 68.1 ± 5.80 nmol/L). Then we proceeded to evaluate its inhibitory activities against other phosphatases (Table 7). The results suggested that TK-642 showed notable selectivity toward SHP2 over SHP2^{PTP}, SHP1 and PTP1B, with IC₅₀ values > 100 μmol/L. Collectively, these findings strongly supported the conclusion that TK-642 served as a highly potent, and selective allosteric SHP2 inhibitor.

2.4. TK-642 is a reversible, non-competitive allosteric SHP2 inhibitor

To characterize the binding property of TK-642, a jump dilution experiment was conducted to confirm the reversibility of compounds. The irreversible compound cryptotanshinone and the reversible compound SHP099 were used as negative and positive controls, respectively. Dilution results revealed that the dephosphorylation activity of SHP2 rapidly recovered after dilution in both the TK-642 and SHP099 groups, whereas the enzyme activity remained largely unaffected in the presence of cryptotanshinone (Fig. 3A). These findings indicated that TK-642 could bind to SHP2 in a reversible manner.

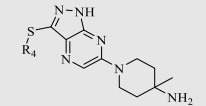
To further elucidate the inhibition mechanism of TK-642, we performed a steady-state kinetics assay *via* varying both inhibitors and substrate concentrations to determine the binding kinetics values for *V*_{max} and *K*_M. As depicted in Fig. 3B–C, the classical Lineweaver-Burk plots intersected at a point along the *x*-axis spanning a spectrum of inhibitor concentrations in both the TK-642 and SHP099 groups. Moreover, *V*_{max} decreased and *K*_M increased curvilinearly with the increase in inhibitor concentration (Table 8). These results demonstrated that TK-642 functioned as a

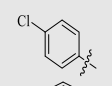
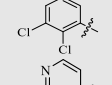
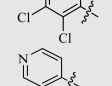
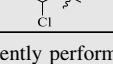
Table 4 Inhibitory effects of compounds **13a–13d** against SHP2^a.


Compd.		SHP2 ^{WT} IC ₅₀ (μmol/L)	SHP2 ^{WT} Δ <i>T</i> _m (°C)
SHP099	—	0.071 ± 0.001	4.370 ± 0.180
13a		>10	N.D. ^b
13b		>10	N.D.
13c		1.145 ± 0.024	2.870 ± 0.080
13d		0.189 ± 0.004	2.260 ± 0.330

^aAll experiments were independently performed at least three times, the data are represented as the mean values.

^bN.D. means not determined.

Table 5 Inhibitory effects of compounds **13e–13h** against SHP2^a.


Compd.	R ₄	SHP2 ^{WT} IC ₅₀ (μmol/L)	SHP2 ^{WT} Δ <i>T</i> _m (°C)
SHP099	—	0.071 ± 0.001	4.370 ± 0.180
13e		0.114 ± 0.001	4.680 ± 0.030
13f		0.013 ± 0.001	7.040 ± 0.110
13g		0.023 ± 0.001	7.660 ± 0.040
13h		0.011 ± 0.001	8.820 ± 0.060

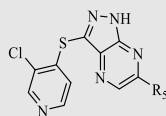
^aAll experiments were independently performed at least three times, the data are represented as the mean values.

substrate-noncompetitive allosteric SHP2 inhibitor. To further confirm the binding preferences of TK-642, the interaction constant α was calculated as previously reported⁴⁸. The observed inverse correlation between V_{\max} and K_M implied that TK-642 ($\alpha = 1.56 \pm 0.01$) exhibited much stronger affinity for free SHP2 protein in comparison with the SHP2/DiFMUP complex, as indicated by an interaction constant $\alpha > 1$ (Table 8). A similar conclusion was also observed in the SHP099 group ($\alpha = 2.49 \pm 0.16$). Therefore, TK-642 can be categorized as a reversible, noncompetitive allosteric SHP2 inhibitor that employed a conformational selection mechanism.

2.5. TK-642 may bind at the “tunnel”-like allosteric pocket of SHP2

Docking simulations predicted the existence of three distinct types of allosteric regulation sites, including “tunnel”-like

allosteric site 1 (e.g., SHP099, TNO155 and BBP-398), “latch”-like allosteric site 2 (e.g., SHP244), and “groove”-like allosteric site 3. Dual inhibition assay aids in identifying the binding mode by evaluating the relationship between two compounds, as indicated by an interaction constant α' ^{29,49}. This analysis can unveil various types of interactions, including synergistic ($0 < \alpha' < 1$), antagonistic ($\alpha' > 1$), independent ($\alpha' = 1$) or exclusive ($\alpha' = \infty$) interactions. Following this principle, dual inhibition biochemical studies were performed to predict the potential binding pocket of TK-642 through a cross titration of TK-642 and SHP099. As shown in Fig. 4, the apparent IC₅₀ (IC₅₀^{app}) of SHP099 exhibited a linear increase with the increasing concentration of TK-642, following the linear equation $Y = 459.1X + 118.4$ ($R^2 = 0.9612$). This result implied a mutually exclusive relationship between TK-642 and SHP099, a well-known inhibitor binding at the “tunnel” allosteric site 1 of SHP2. Consequently, we hypothesized that TK-

Table 6 Inhibitory effects of compounds **13i** and **13j** against SHP2^a.

Compd.	R ₅	SHP2 ^{WT} IC ₅₀ (μmol/L)	SHP2 ^{WT} ΔT _m (°C)
13i (TK-642)		0.0027 ± 0.0001	8.830 ± 0.110
13j		0.0549 ± 0.002	5.080 ± 0.050

^aAll experiments were independently performed at least three times, the data are represented as the mean values.

Table 7 Selectivity profiling of TK-642 against a panel of phosphatases.

Phosphatase	Protein sequence	IC ₅₀ (μmol/L)
SHP2 ^{PTP}	237–535	>100
SHP1	2–595	>100
PTP1B	2–435	>100

642 may competitively bind to the same “tunnel”-like allosteric pocket in SHP2 as SHP099.

A molecular docking study was conducted to further elucidate the potential binding mode of TK-642 with SHP2. As depicted in Fig. 5, TK-642 occupied the “tunnel” site at the interface of the N-SH2, C-SH2 and PTP domains, effectively entrapping SHP2 in an auto-inhibited, inactive conformation. The pyrazine nitrogen in TK-642 formed a hydrogen bond with residue R111 in SHP2, simultaneously maintaining a cation-π interaction with the 3-chloropyridine ring. The terminal basic amine of piperidine ring in TK-642 established an H-bonding interaction with T108. Additionally, the newly introduced aryl-S-bicyclo bridge in TK-642 induced a shift of the 3-chloropyridine group, facilitating its extension into a hydrophobic pocket consisting of residues P491, K492 and Q495. Particularly, both the pyrazine N-atom and the pyrazole NH of TK-642 engaged in H-bonding interactions with E250, endowing TK-642 with the property of “bidentate ligand”. In summary, the binding mode of TK-642 exhibited a favorable shape complementarity to the “tunnel” allosteric binding pocket of SHP2, which agreed well with the observed high potency of TK-642.

2.6. TK-642 inhibits cell proliferation and induces apoptosis of esophageal cancer cells in vitro

The cellular thermal shift assay (CETSA) was performed to investigate the potential of TK-642 in targeting intracellular SHP2 protein. As illustrated in Fig. 6A, a significantly higher expression level of SHP2 protein was observed within the temperature range of 45–63 °C in EGFR amplified KYSE-520 esophageal cancer cell lines treated with TK-642, as compared to the DMSO treatment group. This finding indicated that TK-642 could effectively

bind to and enhance the thermal stability of intracellular SHP2 protein in KYSE-520 cells.

Considering the well-known oncogenic roles of SHP2 in the development of esophageal cancer, we proceeded to investigate the impact of TK-642 on cell proliferation and apoptosis of KYSE-520 cell lines, with SHP099 serving as a control. The results revealed that both compounds exhibited moderate effects on the proliferation of KYSE-520 cells. Especially, the inhibitory activity of TK-642 on the KYSE-520 cells (IC₅₀ = 5.73 ± 0.34 μmol/L) was approximately 3-fold greater than that of SHP099 (IC₅₀ = 15.48 ± 4.18 μmol/L, Fig. 6B). Moreover, we also verified the anti-tumor activity of TK-642 in non small cell lung cancer H1975 and gastric cancer HGC-27 cells. IC₅₀ values of TK-642 in H1975 and HGC-27 cells were 6.68 ± 1.28 and 4.83 ± 1.13 μmol/L, respectively (Fig. 6C). Similar to SHP099, TK-642 also induced the apoptosis of KYSE-520 cells in a concentration-dependent manner (Fig. 6D).

2.7. TK-642 inhibits the SHP2-mediated AKT and ERK signaling pathways

SHP2 plays pivotal roles in various critical intracellular oncogenic signaling pathways, including PI3K-AKT and RAS-RAF-MEK-ERK. To elucidate the underlying mechanism of TK-642, we examined changes in the expression levels of SHP2 downstream effectors after TK-642 treatment, using SHP099 as a control. Our findings revealed that both compounds concentration-dependently suppressed the phosphorylation levels of AKT and ERK1/2 in KYSE-520 cell lines (Fig. 6E). These results indicated that TK-642 can inhibit SHP2-mediated AKT and ERK signaling pathways by diminishing the phosphatase activity of SHP2.

2.8. Liver microsomal stability and pharmacokinetic property of TK-642

Impressed by the overall profile of TK-642, we further evaluated its liver microsomal stability in both humans and mice, using SHP099 and diclofenac (a nonsteroidal anti-inflammatory drug) as reference compounds. In comparison to diclofenac, TK-642 exhibited much lower intrinsic clearance and a longer half-life

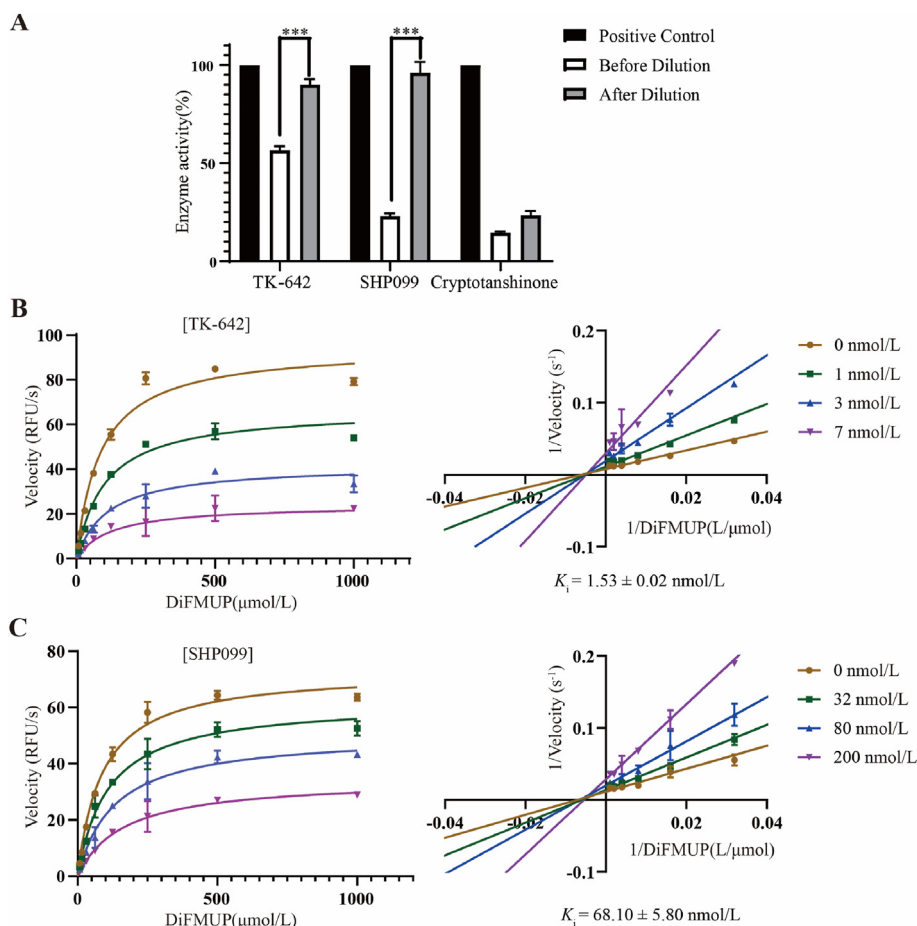


Figure 3 TK-642 is a reversible and noncompetitive allosteric SHP2 inhibitor. (A) The reversibility of TK-642 was identified by the jump dilution assay with the irreversible inhibitor cryptotanshinone and reversible inhibitor SHP099 as controls. (B–C) The inhibition modalities of TK-642 (B) and SHP099 (C) were characterized by steady state kinetics analysis.

Table 8 The reciprocal effect of TK-642 and SHP099 on the apparent parameters of steady state kinetic constants^a.

TK-642	0 nmol/L	1 nmol/L	3 nmol/L	7 nmol/L
V_{\max} (s^{-1})	95.63 ± 0.33	64.92 ± 1.60	41.96 ± 2.36	26.27 ± 3.42
K_M ($\mu\text{mol/L}$)	88.12 ± 0.31	98.51 ± 2.51	118.4 ± 1.8	123.4 ± 7.55
α	1.56 ± 0.01			
SHP099	0 nmol/L	32 nmol/L	80 nmol/L	200 nmol/L
V_{\max} (s^{-1})	74.61 ± 0.04	58.88 ± 0.80	51.63 ± 0.85	34.07 ± 0.92
K_M ($\mu\text{mol/L}$)	89.00 ± 3.31	94.52 ± 4.42	140.23 ± 1.63	153.87 ± 4.26
α	2.49 ± 0.16			

^aRaw data shown as mean ± SD ($n \geq 3$) were fitted to the Michaelis–Menten equation to extrapolate V_{\max} and K_M values.

in liver microsomes of both humans and mice ($CL_{\text{int}} = 34.0$ and 8.71 mL/min/kg, $t_{1/2} = 36.7$ and 630 min). Even though SHP099 also exhibited low microsomal clearance in mice ($CL_{\text{int}} = 20.6$ mL/min/kg), it displayed minimal clearance in human liver microsome (Table 9). These findings underscored the favorable *in vitro* stabilities of TK-642.

To investigate the potential *in vivo* efficacy of TK-642, we conducted a comprehensive evaluation of its pharmacokinetic

(PK) profile. As detailed in Table 10, TK-642 exhibited an excellent PK profile in male SD rats ($n = 3$) at a low dose (2 mg/kg iv, 10 mg/kg po, suspension formulation). The analysis revealed low intrinsic clearance (13.4 ± 1.65 L/h/kg), a favorable half-life ($t_{1/2} = 2.47$ h) and an optimal volume of distribution ($AUC = 411 \pm 24.9$ h·ng/mL po, 151.0 ± 19.0 h·ng/mL iv). Additionally, it exhibited a substantial peak plasma concentration ($C_{\text{max}} = 142 \pm 51.8$ ng/mL)

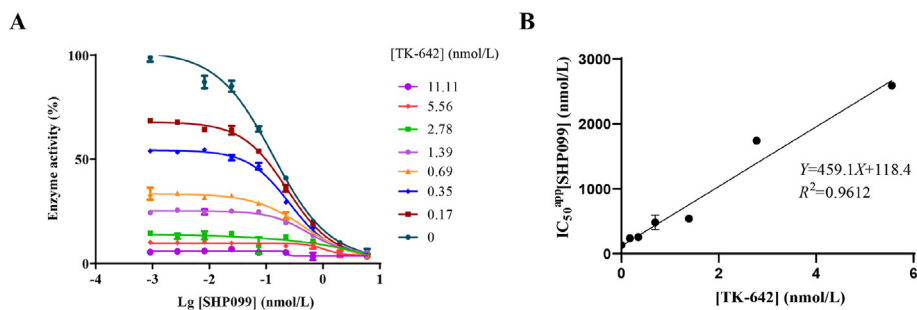


Figure 4 TK-642 may competitively bind at the same allosteric pocket as SHP099 identified by dual inhibition assay. (A) Dual inhibition of SHP2 by TK-642 and SHP099. (B) Mutual exclusive relationship between TK-642 and SHP099.

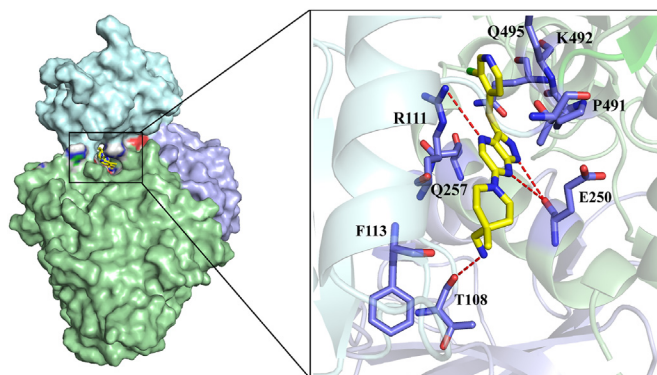


Figure 5 The proposed binding mode of TK-642 with SHP2 (PDB code: 5EHR). The N-SH2 domain of SHP2 is colored in lightblue, the C-SH2 domain is colored in palecyan and the PTP domain is colored in palegreen. TK-642 is displayed in yellow stick representation correspondingly. The hydrogen bond interactions between TK-642 and SHP2 are indicated by the red dashed lines.

and noteworthy oral bioavailability ($F = 42.5 \pm 3.4\%$). Encouraged by these results, we proceeded to investigate its *in vivo* anti-tumor efficacy.

2.9. TK-642 suppresses tumor growth of esophageal cancer *in vivo*

The *in vivo* efficacy of TK-642 was evaluated in mice with subcutaneously implanted KYSE-520 carcinoma cells. Tumor-bearing mice were administered a single oral dose of TK-642 at 50 mg/kg, with SHP099 and saline solution as control groups. As depicted in Fig. 7A–B, a significant anti-tumor effect for both TK-642 and SHP099 was revealed when compared to the saline control. Particularly, TK-642 demonstrated a superior anti-tumor effect compared to SHP099 at the same dosage (Fig. 7A–B). The tumor growth inhibition (TGI) of TK-642 and SHP099 showed significant difference with values of $83.69 \pm 10.44\%$ and $52.28 \pm 18.99\%$, respectively (Fig. 7C). All treatment groups displayed excellent tolerance, with no observable weight loss or other abnormal conditions during treatment (Fig. 7D). To verify the safety profiles of TK-642, we also used CCK8 assay to test the cell growth inhibition activity of TK-642 against 293T cells. Results showed that IC_{50} values of TK-642 in 293T cells was $18.26 \pm 1.62 \mu\text{mol/L}$ (Fig. 7E). Additionally, histopathological analysis revealed no apparent abnormality in the heart, liver,

spleen, lung, and kidney after treatment, indicating that both TK-642 and SHP099 treatments induced minimal damage to these tissues (Fig. 7F).

2.10. Chemistry

In this work, we initially synthesized 12 derivatives of compound **6a** (compounds **6b–6k**), to explore the impact of modifications at the terminal amine moiety. The synthesis of these compounds was illustrated in Schemes 1A, 5-bromo-2,4-dichloropyrimidine (**1**) reacted with 2,3-dichlorobenzaldehyde (**2**) and isopropylmagnesium chloride (Grignard reagent) in anhydrous THF, leading to the formation of the secondary alcohol **3** through nucleophilic addition. This intermediate was further oxidized with Dess-Martin periodinane (DMP) to produce the corresponding ketone **4**. Subsequently, compound **5** was obtained through the cyclization of **4** with hydrazine hydrate. With **5** in hand, a nucleophilic substitution reaction was performed with the appropriate amine in the presence of *N,N*-diisopropylethylamine (DIPEA), giving compounds **6e**, **6f**, and **6i**. Finally, a deprotection step using trifluoroacetic acid (TFA) in CH_2Cl_2 yielded compounds **6a–6d**, **6g–6h**, and **6j–6k**. Similarly, compounds **8a–8s** were also obtained through nucleophilic addition, oxidation, cyclization, nucleophilic substitution, and final deprotection with TFA as well as neutralization with saturated sodium bicarbonate

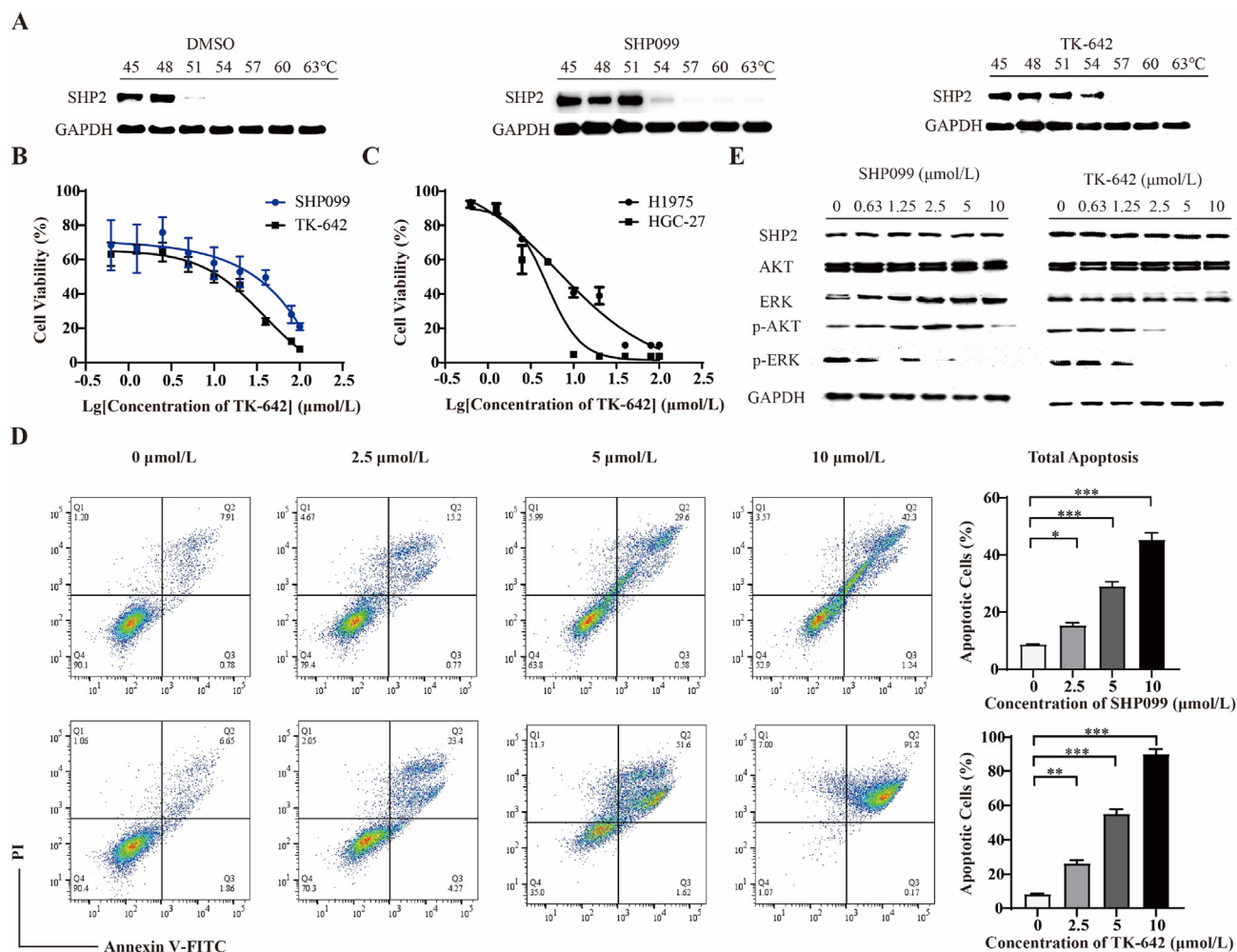


Figure 6 TK-642 inhibits cell proliferation and induces apoptosis of esophageal cancer cells *via* suppressing SHP2-mediated AKT and ERK signaling pathways. (A) CETSA results. KYSE-520 cells were treated with 10 $\mu\text{mol/L}$ TK-642, SHP099 or DMSO for 3 h, subsequently the expression levels of SHP2 and GAPDH were detected by Western blot. All experiments were independently performed three times. (B) Effect of TK-642 on cell proliferation of esophageal cancer cells. KYSE-520 cells were treated with TK-642 or SHP099 at corresponding concentrations (0, 0.625, 1.25, 2.5, 5, 10, 20, 40, 80 and 100 $\mu\text{mol/L}$) for 96 h. Cell numbers were determined using the lactate dehydrogenase WST-8 assay kit. (C) Effect of TK-642 on cell proliferation of non small cell lung cancer H1975 and gastric cancer HGC-27 cells. H1975 and HGC-27 cells were treated with TK-642 at corresponding concentrations (0, 0.625, 1.25, 2.5, 5, 10, 20, 40, 80 and 100 $\mu\text{mol/L}$) for 96 h. Cell numbers were determined using the lactate dehydrogenase WST-8 assay kit. (D) Effect of TK-642 on apoptosis of esophageal cancer cells. KYSE-520 cells were treated with SHP099 or TK-642 at 0, 2.5, 5 and 10 $\mu\text{mol/L}$ for 48 h. Apoptotic cells were then quantified by flow cytometry using the Annexin V staining kit. All experiments were performed at least three times independently, and data were expressed as mean \pm standard deviation. (E) TK-642 inhibits SHP2-mediated AKT and ERK signaling pathways. KYSE-520 cells were treated with DMSO or the indicated concentrations (0, 0.625, 1.25, 2.5, 5, 10 $\mu\text{mol/L}$) of SHP099 and TK-642, and the expression levels of SHP2, p-AKT, AKT and p-ERK, ERK, GAPDH were detected. All experiments were independently performed three times. Student's *t*-test for statistically significant differences. * $P < 0.05$, ** $P < 0.01$, *** $P < 0.001$.

Table 9 Liver microsomal stability of test compounds.

Compd.	Species	$t_{1/2}$ (min)	CL_{int} (mL/min/kg)
Diclofenac	Human	7.15	174
SHP099		>720	0.00
TK-642		36.7	34.0
Diclofenac	Mouse	60.8	90.3
SHP099		267	20.6
TK-642		630	8.71

Table 10 Pharmacokinetics of TK-642 in male SD rats.

PK parameter	<i>po</i> (10 mg/kg)	<i>iv</i> (2 mg/kg)
Sex	M	M
CL (L/h/kg)	ND	13.4 ± 1.65
V_{ss} (L/kg)	ND	11.5 ± 2.28
$t_{1/2}$ (h)	2.47 ± 1.05	0.935 ± 0.139
T_{max} (h)	0.083 ± 0.00	ND
C_{max} (ng/mL)	142 ± 51.8	ND
AUC (h·ng/mL)	411 ± 24.9	151.0 ± 19.0
F (%)	42.5 ± 3.4	

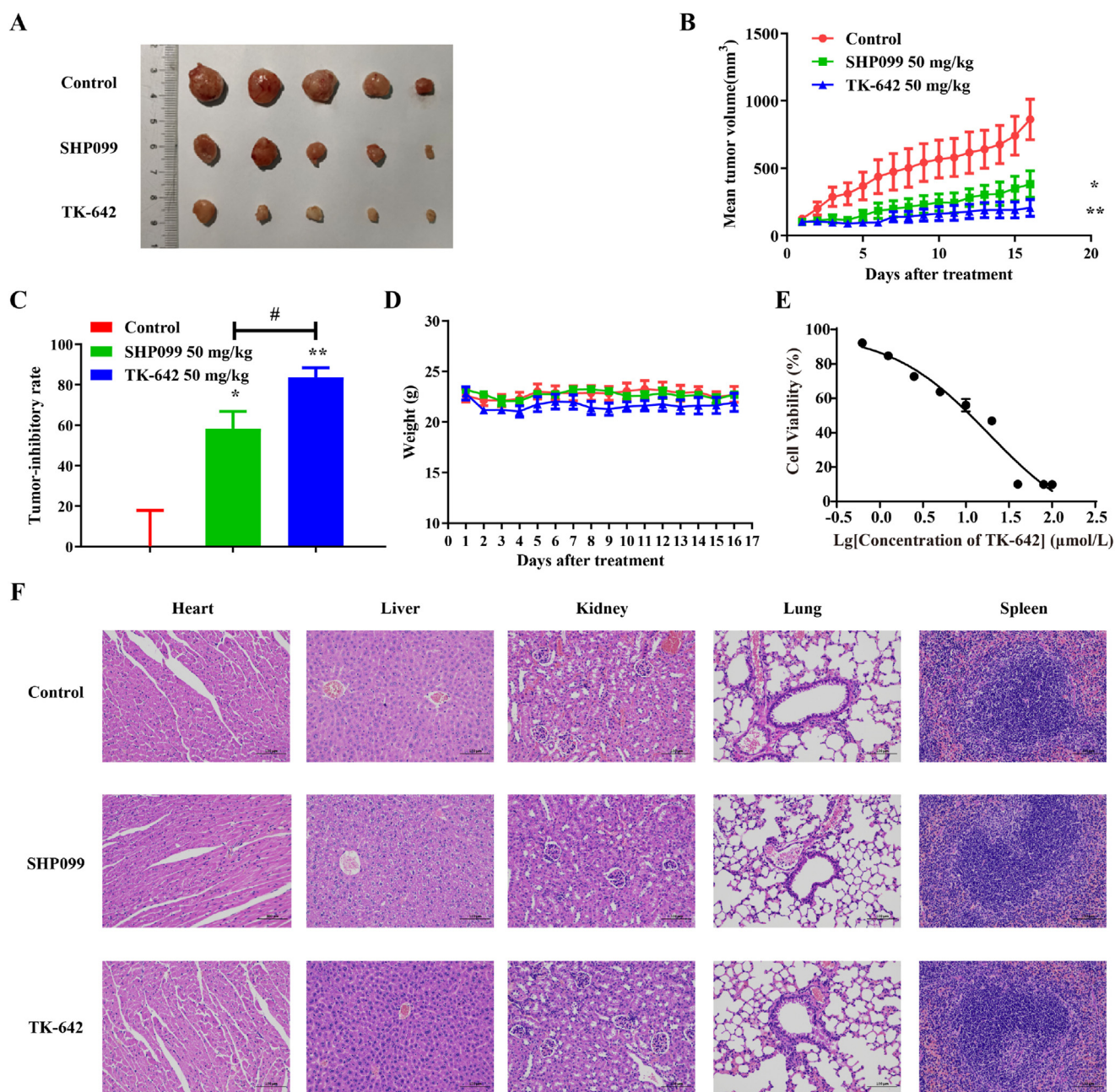


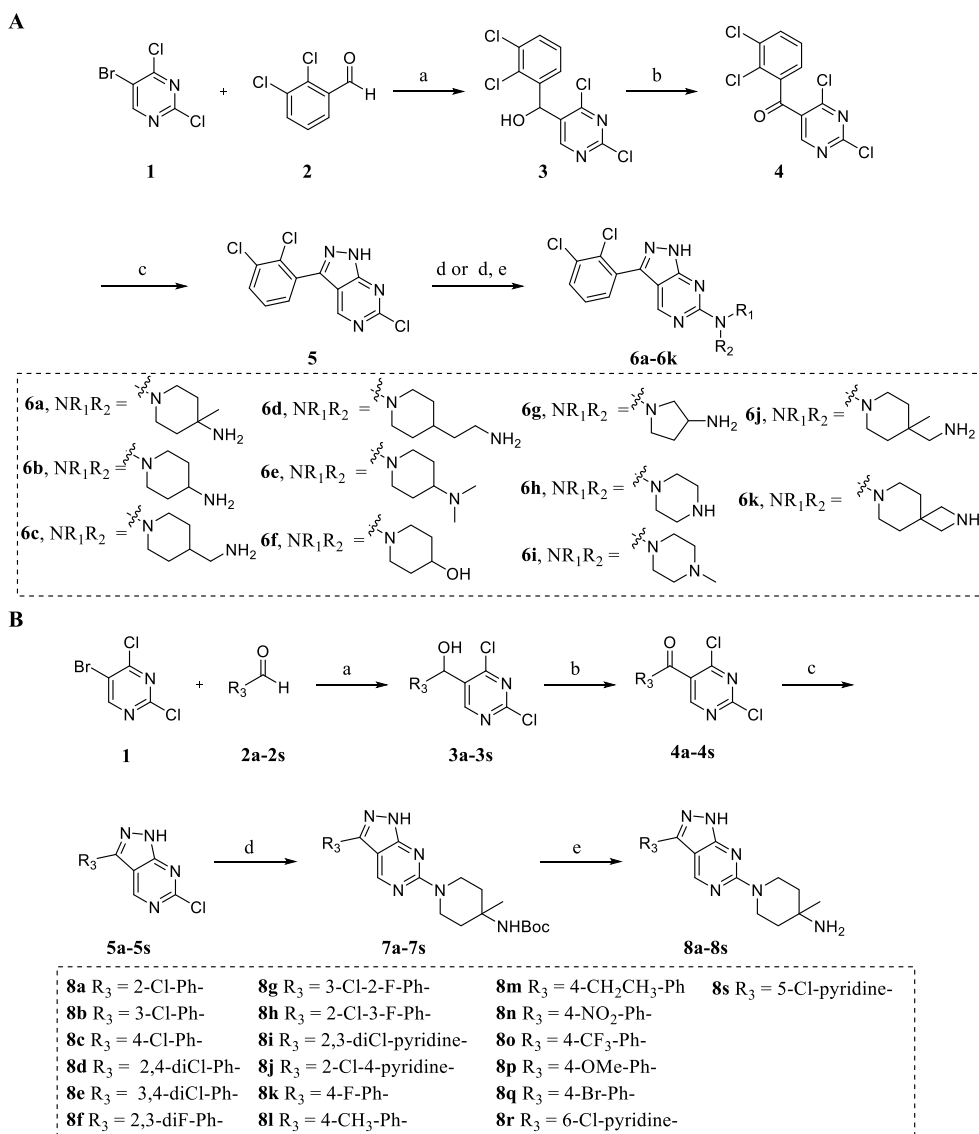
Figure 7 Anti-tumor efficacy of TK-642 and SHP099 in KYSE-520 xenograft esophageal cancer models. (A) The tumor size recorded on day 16 post-treatment. (B) Mean tumor volume at various time points. (C) The tumor growth inhibitory rate. (D) Changes in mouse body weight during the treatment period. (E) Effect of TK-642 on cell proliferation of 293T cells. 293T cells were treated with TK-642 at corresponding concentrations (0, 0.625, 1.25, 2.5, 5, 10, 20, 40, 80 and 100 $\mu\text{mol/L}$) for 96 h. Cell numbers were determined using the lactate dehydrogenase WST-8 assay kit. (F) Representative images of H&E-stained tissues. * $P < 0.05$, ** $P < 0.01$ vs Control. ## $P < 0.01$ TK-642 vs SHP099.

solution, under nearly identical reaction conditions as described in Scheme 1B.

As shown in Scheme 2A, we initiated the synthesis process by the bromination of commercially available materials **9a–9d** with *N*-bromosuccinimide (NBS) to yield intermediates **10a–10d**. These intermediates were then subjected to a nucleophilic aromatic substitution (S_NAr) reaction with *tert*-butyl 4-methylpiperidin-4-ylcarbamate, resulting in intermediates **11a–11d**. Subsequently, treatment of **11a–11d**

with 4-chlorophenylboronic acid via the Pd-catalyzed Suzuki–Miyaura reaction produced the corresponding intermediates **12a–12d**. These intermediates were further deprotected with trifluoroacetic acid (TFA) to yield the final products **13a–13d**.

Compounds **13e–13h** were synthesized by the iodination of 6-chloro-1*H*-pyrazolo[3,4-*b*]pyrazine (**9d**) using *N*-iodosuccinimide (NIS), as described in Scheme 2B. Subsequently, the *tert*-butyl 4-methylpiperidin-4-ylcarbamate group was introduced, yielding



Scheme 1 Synthesis of compounds **6a–6k** and **8a–8s**. Reagents and conditions: (a) Grignard reagent, anhydrous THF, -78°C , 5 h; (b) DMP, CH_2Cl_2 , r.t., 12 h; (c) hydrazine hydrate, THF, r.t., 6 h; (d) appropriate amines, DIPEA, CH_3CN , 80°C , 6 h; (e) TFA, CH_2Cl_2 , r.t., 2 h.

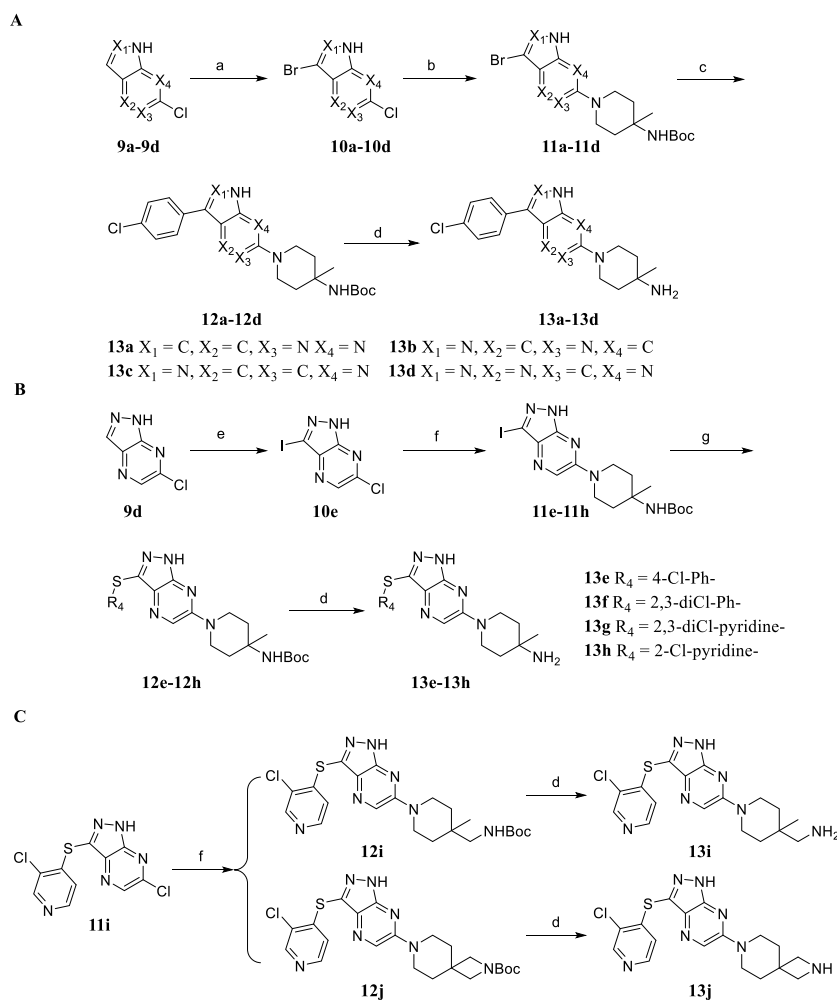
intermediates **11e–11h**. The next step involved a CuI-mediated coupling of the appropriate thiophenols to intermediates **11e–11h**, and final deprotection of the Boc group provided the desired compounds **13e–13h**.

Particularly, compounds **13i** and **13j** were obtained following the procedure outlined in Scheme 2C. The $\text{S}_{\text{N}}\text{Ar}$ reaction of first coupling intermediate **11i** with the *tert*-butyl ((4-methylpiperidin-4-yl)methyl)carbamate and *tert*-butyl 2,7-diazaspiro[3.5]nonane-2-carboxylate yielded intermediates **12i** and **12j**, respectively. Finally, the Boc-deprotection with TFA generated products **13i** and **13j**.

3. Conclusions

Starting from the hit compound TK-145 identified from our compound library, we performed further structure-guided design

by merging the 4-amine of pyrimidine ring and the adjacent 5-carbon into a bicyclic skeleton, leading to the generation of a series of fused bicyclic-based allosteric SHP2 inhibitor. TK-642 emerged as a potent SHP2 inhibitor, showing reversible, substrate noncompetitive inhibition of the phosphatase activity of SHP2 (SHP2^{WT} IC₅₀ = 2.7 ± 0.1 nmol/L) and high selectivity over a panel of phosphatases. TK-642 likely bound at the “tunnel” allosteric site of SHP2. In cellular assays, TK-642 could effectively suppress cell proliferation (KYSE-520 cells IC₅₀ = 5.73 ± 0.34 $\mu\text{mol/L}$) and induce apoptosis of esophageal cancer cells through inhibiting the SHP2-mediated AKT and ERK signaling pathways. *In vivo* studies indicated that TK-642 possessed significant anti-tumor efficacy, as demonstrated by a T/C value of $83.69 \pm 10.44\%$ when administered orally at a dosage of 50 mg/kg in the KYSE-520 xenograft mouse model. In light of its potency, selectivity, and favorable oral bioavailability,



Scheme 2 Synthesis of compounds **13a–13j**. Reagents and conditions: (a) NBS, DMF, r.t., 1 h; (b) *tert*-butyl (piperidin-4-ylmethyl)carbamate, DIPEA, DMSO, 120 °C, 4 h; (c) 4-chlorophenylboronic acid, PdCl₂(dppf), K₂CO₃, MeCN/H₂O (5:1), 100 °C, degassed, 5 h; (d) TFA, DCM, r.t., 2 h; (e) NIS, DMF, r.t., 1 h; (f) *tert*-butyl (piperidin-4-ylmethyl)carbamate, DIPEA, DMSO, 120 °C, 4 h; (g) appropriate thiophenol, CuI, K₂CO₃, 1,10-phenanthroline, 1,4-dioxane, 100 °C, degassed, 6 h.

TK-642 is worthy of further investigation as a promising lead compound in preclinical studies.

4. Experimental

4.1. (1-(3-((3-Chloropyridin-4-yl)thio)-1H-pyrazolo[3,4-b]pyrazin-6-yl)-4-methylpiperidin-4-yl)methanamine (**13i**)

White solid, m.p. 208.5–209.2 °C, yield 38.2%. HPLC purity: 97.20%. ¹H NMR (400 MHz, DMSO-*d*₆) δ 8.56 (s, 1H), 8.47 (s, 1H), 8.19 (d, *J* = 5.3 Hz, 1H), 6.64 (d, *J* = 5.3 Hz, 1H), 4.08–3.95 (m, 2H), 3.60–3.52 (m, 2H), 2.73 (s, 2H), 1.65–1.57 (m, 2H), 1.51–1.40 (m, 2H), 1.07 (s, 3H). ¹³C NMR (100 MHz, DMSO-*d*₆) δ 153.28, 148.15, 147.72, 146.64, 145.25, 132.48, 130.23, 126.99, 124.50, 120.85, 48.62, 33.26, 31.77, 21.24. HRMS (ESI): *m/z* calcd for C₁₇H₂₁ClN₇S [M+H]⁺ 390.1268; found 390.1265.

The synthesis and characterization data of other compounds are provided in the Supporting Information.

4.2. Protein expression and purification

PTPN11 gene coding sequences, encompassing SHP2^{WT} (1–535 aa) and SHP2^{PTP} (237–535 aa), were inserted into pET-28a (+) plasmid and subsequently transformed into BL21 Rosetta (DE3) *E. coli* cells. The bacterial culture was incubated at 37 °C in Luria Broth (LB) medium supplemented with 34 mg/L kanamycin and 25 mg/L chloramphenicol. Cells were induced with 0.3 mmol/L isopropyl-*D*-thiogalactopyranoside (IPTG, Sangon Biotech, cat. 367-93-1) and harvested following overnight growth at 16 °C.

Cells were resuspended in lysis buffer [20 mmol/L Tris-HCl pH 8.5, 300 mmol/L NaCl, 10 mmol/L β-mercaptoethanol and 2.5 mmol/L phenylmethane sulfonyl fluoride (PMSF)], lysed by sonication and then centrifuged at 12,000 rpm for 75 min. Cell

supernatants were incubated with Ni²⁺-NTA agarose resin (QIAGEN, cat. 1018240) for 1 h at 4 °C. Following washing with lysis buffer, the target proteins were collected with elution buffer (20 mmol/L Tris-HCl pH 8.5, 300 mmol/L NaCl, 10 mmol/L β-mercaptoethanol and 2.5 mmol/L PMSF, 200 mmol/L imidazole). Protein was subsequently diluted and applied to a HiTrap™ Q HP chromatography column (GE healthcare) equilibrated with 20 mmol/L Tris, pH 8.5, 0 or 1 mol/L NaCl, 2.2 mmol/L DTT. The target protein was eluted with a 25-column volume gradient from 0 to 1 mol/L NaCl. Fractions containing SHP2 protein were pooled and concentrated, and then loaded onto a Superdex™ 200 Increase 10/300 GL column (GE Healthcare). Finally, the recombinant SHP2 proteins were collected and stored at −80 °C.

4.3. Cross-validation high-throughput screening assay

The screening procedure was conducted as our previously described in our published work⁴⁶. The *in vitro* SHP2^{WT} dephosphorylation enzyme reaction system contained 0.5 nmol/L SHP2^{WT} protein, 1.0 μmol/L p-IRS1 peptide, and various compound concentrations ranging from 0.0003 to 10 μmol/L. After 1 h incubation at room temperature, 10 μmol/L DiFMUP was added into the system. The buffer conditions included 60 mmol/L HEPES pH 7.2, 75 mmol/L NaCl, 75 mmol/L KCl, 1 mmol/L EDTA, 0.05% Tween-20 and 5 mmol/L DTT. The enzyme velocity was measured by monitoring changes in fluorescence signals using a multimode plate reader (PerkinElmer Enspire) configured with an excitation wavelength of 350 nm and an emission wavelength of 450 nm. Relative fluorescence intensity (FI) was determined by subtracting the initial (0 min) FI value from the ending (30 min) FI value. Subsequently, dose–response curves for the inhibitors were plotted using normalized IC₅₀ regression curve fitting, with control-based normalization to extrapolate IC₅₀ values.

The *in vitro* SHP2^{PTP} dephosphorylation enzyme reaction system was set as 20 μL containing 0.14 nmol/L SHP2^{PTP} protein and different concentrations of compounds (ranging from 0.1 to 50 mmol/L) followed by addition of 100 mmol/L DiFMUP after 30 min pre-incubation. The inhibition potency of test compounds against SHP2^{PTP} was also measured as the above procedure.

The thermal shift assay system was established with 2 μL of 1.8 μmol/L SHP2^{WT} protein, 2 μL of 7.5 × SYPRO orange dye and 2 μL of 100 μmol/L compounds, or 1% DMSO as control. The assay buffer contained 100 mmol/L Bis-Tris pH 6.5, 100 mmol/L NaCl and 1 mmol/L DTT. The raw data acquired using Real-Time PCR (Quantstudio™6 Flex System, Thermo Fisher Scientific) were then analyzed by fitting them to the Boltzmann sigmoidal equation. This analysis provided the melting temperature (T_m) and variance in T_m (ΔT_m) between apo-SHP2 and SHP2/compound complexes.

Compounds that displayed inhibitory activity against SHP2^{WT} rather than SHP2^{PTP}, and induced change in melting temperature were finally identified as allosteric SHP2 inhibitors.

4.4. Selectivity analysis

The selectivity assay against various PTPs, such as SHP1 and PTP1B, was conducted following the similar dephosphorylation enzyme assay described above. The DiFMUP concentrations were determined based on the K_M value for each specific phosphatase.

4.5. Reversibility analysis

50 nmol/L SHP2^{WT} protein was preincubated with candidate compound TK-642 (8-fold IC₅₀ concentrations), positive control SHP099 (20-fold IC₅₀ concentrations) or negative control cryptotanshinone (20-fold IC₅₀ concentrations) for 30 min at room temperature. Then 2 μL aliquot was extracted from the mixture and introduced into a 200 μL substrate buffer containing 1.0 μmol/L p-IRS1 and 10.0 μmol/L DiFMUP. The fluorescence values was continuously monitored using a multimode plate reader with an excitation wavelength of 350 nm and an emission wavelength of 450 nm. The inhibitory rate recovery of compounds after jump dilution was normalized by comparing it to the DMSO control. It was anticipated that irreversible inhibitor would have minimal impact on the inhibitory rate recovery of SHP2 phosphatase activity, while the inhibitory rate recovery of reversible inhibitor exhibited statistically significant changes.

4.6. Steady state kinetics analysis

0.5 nmol/L SHP2^{WT} protein was pre-incubated with 1.0 μmol/L 2p-IRS1 and varying concentrations of candidate compound TK-642 (0, 1, 3 and 7 nmol/L) or the control SHP099 (0, 32, 80 and 200 nmol/L) at room temperature. After 1 h, the reaction was initiated by introducing different concentrations of the substrate DiFMUP, ranging from 2 μmol/L to 1000 μmol/L. The fluorescence values was continuously monitored using a multimode plate reader with an excitation wavelength of 350 nm and an emission wavelength of 450 nm. The kinetic parameters were determined through Lineweaver-Burk plots and noncompetitive analysis *via* Eq. (1):

$$V = \frac{V_{\max} [S]}{[S] \left(1 + \frac{[I]}{\alpha K_i} \right) + K_M \left(1 + \frac{[I]}{K_i} \right)} \quad (1)$$

where I is the concentration of candidate compounds, S is the concentration of substrate, V_{\max} is the maximal enzyme velocity, V is the fractional velocity in the presence of varying concentration of inhibitor, K_M is the Michaelis–Menten constant, K_i is the dissociation constant of candidate compounds, α is the interaction constant as a symbol of the affinity difference between candidate compounds and the free enzyme or enzyme–substrate complex.

The enzymatic reaction rate V was calculated for each sample pore, and the trend of V_{\max} and K_M values were analyzed to determine the type of inhibition by plotting the non-linear fitting curve with V as the vertical axis and DiFMUP concentration as the horizontal axis. Meanwhile, the double inverse linear equation was analyzed and fitted with $1/V$ as the vertical axis and $1/[\text{DiFMUP}]$ as the horizontal axis, to determine the type of inhibition based on the characteristics of the double inverse curve equation.

4.7. Dual inhibition biochemical assay

After incubating 0.5 nmol/L SHP2^{WT} protein with 0.1 μmol/L 2p-IRS1 for 5–10 min, a 1:3 concentration gradient dilution of reference compound SHP099 (final concentration ranging from 0.91 to 6000 nmol/L) was added to the mixed system and incubated for 30 min at room temperature. Then a 1:2 concentration gradient dilution of the candidate compound TK-642 (final

concentration ranging from 0.17 to 11.11 nmol/L) or DMSO were dispensed in pairs and incubated at room temperature for 30 min, following by the adding of 10 $\mu\text{mol/L}$ substrate DiFMUP to initiate the dephosphorylation reaction. The progress curve was continuously monitored using a multimode plate reader with excitation and emission wavelengths of 350 nm and 450 nm, respectively. The inhibitor dose–response curves were initially plotted using normalized IC_{50} regression curve fitting, employing control-based normalization to extrapolate IC_{50} values. Subsequently, the apparent IC_{50} ($\text{IC}_{50}^{\text{app}}$) of SHP099 at various concentrations of TK-642 was determined as a function of TK-642 concentration and fitted using the following the dual inhibition Eq. (2):

$$\text{IC}_{50}^J = K_J \left(\frac{1 + \frac{I}{K_I}}{\alpha + \frac{I}{\alpha K_I}} \right) \quad (2)$$

In concern of mutual exclusive relationship, where reference compound and candidate compound occupy the same binding site simultaneously, the parameter α becomes infinite and the dual inhibition equation (2) can be simplified to a linear Eq. (3):

$$\text{IC}_{50}^J = K_J + \left(\frac{K_J}{K_I} \right) I \quad (3)$$

where I is the concentration of candidate compounds, J is the concentration of reference compound, K_I is the dissociation constant of candidate compounds, K_J is the dissociation constant of reference compound, α is the interaction constant as a symbol of the affinity difference between the enzyme and reference compound or candidate compounds. IC_{50}^J is the apparent half inhibitory concentration of reference compound in the presence of varying concentration of I .

4.8. Molecular docking assay

In silico docking analysis was conducted utilizing the Molecular Operating Environment software (MOE, version 2014.09). The SHP2/SHP099 structure (PDB code: 5EHR) was chosen as the receptor structure. The protein model was prepared using the default structure preparation module. The three-dimensional structure of TK-642 was generated through protonation, energy minimization, and conformational searching. Subsequently, the generated conformations of TK-642 were docked into the ligand-binding pockets of SHP2 using the default DOCK module. The program generated 20 ligand poses, scored by London dG and GBVI/WSA dG. After a thorough visual examination, the pose with the highest score was selected as the proposed binding mode of TK-642 with SHP2 to elucidate its binding characteristics.

4.9. Cell lines and cell culture

Esophageal cancer cell line KYSE-520, non small cell lung cancer cells H1975 and gastric cancer cell line HGC-27 were purchased from National Collection of Authenticated Cell Cultures. KYSE-520, H1975 and HGC-27 cell lines were cultured in RPMI-1640 medium supplemented with 10% fetal bovine serum in a 37 °C constant humidity incubator containing 5% CO_2 .

4.10. Cellular thermal shift assay

KYSE-520 cells in logarithmic growth phase were seeded into 10 cm culture dishes. When cell confluence reached approximately 60%–70%, they were treated with DMSO or TK-642 (10 $\mu\text{mol/L}$) for 3 h. Subsequently, the cells were harvested using PBS solution containing protease inhibitor and the samples were heated at gradient temperatures ranging from 45 to 63 °C for 3 min. Afterward, the samples were repeatedly frozen and thawed for 3–5 times using liquid nitrogen to reach -37 °C. The supernatant were collected through centrifuging the samples. Finally, the expression level changes of SHP2 protein were analyzed by Western Blot.

4.11. Cell proliferation assay

Cell viability was evaluated with a WST-8 assay, following the manufacturer's provided guidelines. Cells in logarithmic growth phase (1500 cells/well) were plated onto 96-well plates. Various concentrations of compounds (0.625, 1.25, 2.5, 5, 10, 20, 40, 80 and 100 $\mu\text{mol/L}$) were added 12 h after cell plating. Following a 5-day incubation, 10 μL of WST-8 (meilunbio, cat. MA0218) reagents was added and co-incubated at 37 °C for 1.5–2 h. Luminescent signal was measured at 450 nm. The raw data were normalized to vehicle-treated cells, and IC_{50} values were plotted by non-linear regression analysis with GraphPad Prism 6 software.

4.12. Apoptosis assay

KYSE-520 cells were seeded in 6-well plates for overnight. Cells were then treated with gradient concentration of compounds (0, 2.5, 5 and 10 $\mu\text{mol/L}$) and collected after 48 h. After two-times washing, apoptotic cells were stained with Annexin V APC Apoptosis Assay Kit (MultiSciences, cat. AP101) at 4 °C for 30 min and then quantified by FACS (BD FACS Celesta).

4.13. Western blot

KYSE-520 cells were seeded in 6-well plates overnight and then treated with different concentrations (0.625, 1.25, 2.5, 5, and 10 $\mu\text{mol/L}$) of TK-642 for 2 h, with SHP099 and 0.1% DMSO as controls. The cells were harvested and lysed with RIPA cell lysis buffer containing protease and phosphatase inhibitors. The supernatant of lysed cell suspension was collected. After quantitative analysis, the cell lysates were separated by a 12% SDS-PAGE gel and transferred onto PVDF (polyvinylidene difluoride) membranes. These PVDF membranes were then incubated with the primary antibodies (Rabbit anti-phospho-AKT, anti-AKT, anti-phospho-ERK, anti-ERK and anti-GAPDH monoclonal antibodies) overnight at 4 °C, followed by 2 h incubation with secondary antibodies at room temperature. Finally, the protein bands were visualized using a Western blot detection kit. The ratio of the net protein bands to net loading control was calculated by subtracting the background from the reverse band values.

Antibodies GAPDH (Good Here Technology, cat. AB-P-R001), SHP2 Rabbit monoclonal antibody (Abcam, cat. 32083), AKT (pan) Rabbit monoclonal antibody (Cell Signaling Technology, cat. 4691), phospho-AKT (Ser473) Rabbit monoclonal antibody (Cell Signaling Technology, cat. 4060), p44/42 MAPK (ERK1/2) Rabbit monoclonal antibody (Cell Signaling Technology, cat. 4695) and phospho-p44/42 MAPK (ERK1/2) Rabbit

monoclonal antibody (Cell Signaling Technology, cat. 4370) were used in Western blot assay.

4.14. Liquid chromatography and mass spectrometry conditions

LC-MS/MS analysis of the compounds was performed by LC-MS/MS (Triple Quad 5500+) with a Synergi 4 μm Fusion-RP 80 A LC Column (2×50 mm). The mobile phase was as follows: (A) aqueous phase: 0.1% formic acid in water; (B) organic phase: acetonitrile. The gradient elution was at a flow rate of 0.8 mL/min. Compounds were eluted in the following gradient conditions: the initial proportion was 10% B, and increasing to 95% B in 1 min and hold for 0.2 min, followed by decreasing to 1% B within 0.01 min, and maintained for 0.29 min. The mass spectrometric detection was performed with an electrospray ionization (ESI) source in positive mode. Quantification was acquired by multiple reaction monitoring (MRM) mode of m/z 390.00/354.30 at 0.59 min for TK-642, m/z 352.00/267.00 at 0.62 min for SHP099.

4.15. Metabolic stability

Different species liver microsomes (human, rat, mouse, dog, monkey) were used to evaluate the metabolic stability of TK-642. The *in vitro* metabolic reaction system was composed of phosphate buffer, MgCl_2 and microsomes. The reaction was started with the addition of 30 μL of the 10 mmol/L NADPH. The final concentrations of NADPH was 1 mmol/L. The incubation solution was incubated in water bath at 37 $^\circ\text{C}$. Aliquots of 30 μL were taken from the reaction solution at 0, 5, 15, 30 and 60 min. The reaction was stopped by the addition of 200 μL of cold MeOH:acetonitrile = 1:1 with IS. Samples were centrifuged at 4000 rpm for 10 min.

4.16. Plasma sample preparation

An aliquot of 50 μL plasma sample was added with 500 μL solution (MeOH:acetonitrile = 1:1). The mixture was vortexed for 5 min and centrifuged at 14,800 rpm for 5 min at 4 $^\circ\text{C}$. An aliquot of 5 μL supernatant was injected for qualitative LC-MS/MS analysis.

4.17. Pharmacokinetic assay

SD Rats (223.5–265.1 g, male) were used for pharmacokinetics of TK-642. During overnight fasting prior to dosing and until 4 h post-dose. The rat was restrained manually at the designated time points. About 100 μL of blood samples were taken from the animals *via* jugular vein into micro K2EDTA tubes. Blood samples of 5, 15, 30 min and 1, 2, 4, 8, 24 h were collected and centrifuged at 6000 rpm for 8 min at 4 $^\circ\text{C}$ to generate plasma samples within 0.5 h of collection. Plasma samples were stored at approximately -20 $^\circ\text{C}$ until analysis.

4.18. Efficacy studies in the KYSE-520 xenograft mouse models

All animal experiments were under the guidelines of the Animal Ethics Committee of the School of Pharmacy, Zhengzhou University. Male NU/NU mice weighing 18–22 g were injected subcutaneously with KYSE-520 cells (8×10^6 cells/mouse). when tumors volume reached 100 mm^3 , mice were randomized into

three groups ($n = 5$) and dosed orally with vehicle, SHP099 (50 mg/kg, once a day) and TK-642 (50 mg/kg, once a day) for 16 days, respectively. The tumor size and body weight were measured daily until the last day of the experiment. Tumor volume was calculated as $V = ab^2/2$ (a is the length and b is the width of the tumor). At the end of treatment, all mice were sacrificed and tumor, heart, liver, spleen, lung, kidney tissues were collected.

4.19. Data analysis and statistics

All experiments were conducted in triplicate and the results are presented as mean \pm SD ($n > 3$). Group analysis was carried out using one-way ANOVA to compare the averages of the treated groups with the control group, and a P -value of less than 0.01 was considered to indicate a statistically significant difference.

Acknowledgments

We acknowledge the financial support from the Natural Science Foundation of China (Nos. U21A20416, 32371317, 22277110, and 82104279), Natural Science Foundation of Henan Province (No. 222300420069, China), and “Chunhui Plan” Cooperative Scientific Research Project of the Ministry of Education (No. HZKY20220280, China), State Key Laboratory of Pharmaceutical Biotechnology, Nanjing University (KF-202303, China).

Author contributions

Hong-Min Liu, Yihui Song and Bin Yu as the supervisors conceived the project and supplied the financial support. Kang Tang conducted the synthesis of compounds and supervised the drug-likeness evaluation. Shu Wang, Siqi Feng, Xinyu Yang, Yueyang Guo, Xiangli Ren and Linyue Bai conducted and supervised the biological activity evaluation assay. Molecular docking and molecular dynamics simulation experiment were performed by Kai Tang. Kai Tang, Shu Wang, Siqi Feng and Xinyu Yang conducted the data analysis. Yihui Song, Bin Yu, Kai Tang, Shu Wang and Siqi Feng wrote and revised the manuscript.

Conflicts of interest

The authors declare no competing financial interest.

Appendix A. Supporting information

Supporting information to this article can be found online at <https://doi.org/10.1016/j.apsb.2024.03.028>.

References

1. Liu Q, Qu J, Zhao M, Xu Q, Sun Y. Targeting SHP2 as a promising strategy for cancer immunotherapy. *Pharmacol Res* 2020;**152**:104595.
2. Ostman A, Hellberg C, Böhmer FD. Protein-tyrosine phosphatases and cancer. *Nat Rev Cancer* 2006;**6**:307–20.
3. Zhang J, Zhang F, Niu R. Functions of Shp2 in cancer. *J Cell Mol Med* 2015;**19**:2075–83.
4. Hof P, Pluskey S, Dhe-Paganon S, Eck MJ, Shoelson SE. Crystal structure of the tyrosine phosphatase SHP-2. *Cell* 1998;**92**:441–50.
5. Grossmann KS, Rosário M, Birchmeier C, Birchmeier W. The tyrosine phosphatase Shp2 in development and cancer. *Adv Cancer Res* 2010;**106**:53–89.

6. Song Y, Yang X, Wang S, Zhao M, Yu B. Crystallographic landscape of SHP2 provides molecular insights for SHP2 targeted drug discovery. *Med Res Rev* 2022;**42**:1781–821.
7. Song Y, Yang X, Yu B. KRAS Q61H mutation confers cancer cells with acquired resistance to SHP2 inhibition. *Pharmaceutical Fronts* 2022;**4**:e40–2.
8. Tartaglia M, Niemeyer CM, Fragale A, Song X, Buechner J, Jung A, et al. Somatic mutations in PTPN11 in juvenile myelomonocytic leukemia, myelodysplastic syndromes and acute myeloid leukemia. *Nat Genet* 2003;**34**:148–50.
9. Bentires AM, Paez JG, David FS, Keilhack H, Halmos B, Naoki K, et al. Activating mutations of the noonan syndrome-associated SHP2/PTPN11 gene in human solid tumors and adult acute myelogenous leukemia. *Cancer Res* 2004;**64**:8816–20.
10. Chan G, Kalaitzidis D, Neel BG. The tyrosine phosphatase Shp2 (PTPN11) in cancer. *Cancer Metastasis Rev* 2008;**27**:179–92.
11. Song Y, Zhao M, Zhang H, Yu B. Double-edged roles of protein tyrosine phosphatase SHP2 in cancer and its inhibitors in clinical trials. *Pharmacol Ther* 2021;**230**:107966.
12. Song Y, Yu B. Targeting SHP2 for cancer treatment: advances and prospects. In: Rezaei N, editor. *Handbook of cancer and immunology*. Cham: Springer International Publishing; 2022. p. 1–19.
13. Liu Q, Qu J, Zhao M, Xu Q, Sun Y. Targeting SHP2 as a promising strategy for cancer immunotherapy. *Pharmacol Res* 2020;**152**:104595.
14. Song Y, Wang S, Zhao M, Yang X, Yu B. Strategies targeting protein tyrosine phosphatase SHP2 for cancer therapy. *J Med Chem* 2022;**65**:3066–79.
15. Edouard T, Combiér JP, Nédélec A, Bel-Vialar S, Métrich M, Conte-Auriol F, et al. Functional effects of PTPN11 (SHP2) mutations causing LEOPARD syndrome on epidermal growth factor-induced phosphoinositide 3-kinase/AKT/glycogen synthase kinase 3 β signaling. *Mol Cell Biol* 2010;**30**:2498–507.
16. LaRochelle JR, Fodor M, Vemulapalli V, Mohseni M, Wang P, Stams T, et al. Structural reorganization of SHP2 by oncogenic mutations and implications for oncoprotein resistance to allosteric inhibition. *Nat Commun* 2018;**9**:4508.
17. Pathak MK, Yi T. Sodium stibogluconate is a potent inhibitor of protein tyrosine phosphatases and augments cytokine responses in hemopoietic cell lines. *J Immunol* 2001;**167**:3391–7.
18. Liu W, Yu B, Xu G, Xu WR, Loh ML, Tang LD, et al. Identification of cryptotanshinone as an inhibitor of oncogenic protein tyrosine phosphatase SHP2 (PTPN11). *J Med Chem* 2013;**56**:7212–21.
19. Chen L, Sung SS, Yip ML, Lawrence HR, Ren Y, Guida WC, et al. Discovery of a novel SHP2 protein tyrosine phosphatase inhibitor. *Mol Pharmacol* 2006;**70**:562–70.
20. Hellmuth K, Grosskopf S, Lum CT, Würtele M, Röder N, von Kries JP, et al. Specific inhibitors of the protein tyrosine phosphatase Shp2 identified by high-throughput docking. *Proc Natl Acad Sci U S A* 2008;**105**:7275–80.
21. Grosskopf S, Eckert C, Arkona C, Radetzki S, Böhm K, Heinemann U, et al. Selective inhibitors of the protein tyrosine phosphatase SHP2 block cellular motility and growth of cancer cells *in vitro* and *in vivo*. *ChemMedChem* 2015;**10**:815–26.
22. Lawrence HR, Pireddu R, Chen L, Luo Y, Sung SS, Szymanski AM, et al. Inhibitors of Src homology-2 domain containing protein tyrosine phosphatase-2 (Shp2) based on oxindole scaffolds. *J Med Chem* 2008;**51**:4948–56.
23. Mostinski Y, Heynen GJJE, López-Alberca MP, Paul J, Miksche S, Radetzki S, et al. From pyrazolones to azaindoles: evolution of active-site SHP2 inhibitors based on scaffold hopping and bioisosteric replacement. *J Med Chem* 2020;**63**:14780–804.
24. Yuan X, Bu H, Zhou J, Yang CY, Zhang H. Recent advances of SHP2 inhibitors in cancer therapy: current development and clinical application. *J Med Chem* 2020;**63**:11368–96.
25. Tang K, Jia YN, Yu B, Liu HM. Medicinal chemistry strategies for the development of protein tyrosine phosphatase SHP2 inhibitors and PROTAC degraders. *Eur J Med Chem* 2020;**204**:112657.
26. Chen YN, LaMarche MJ, Chan HM, Fekkes P, Garcia-Fortanet J, Acker MG, et al. Allosteric inhibition of SHP2 phosphatase inhibits cancers driven by receptor tyrosine kinases. *Nature* 2016;**535**:148–52.
27. Garcia Fortanet J, Chen CH, Chen YN, Chen Z, Deng Z, Firestone B, et al. Allosteric inhibition of SHP2: identification of a potent, selective, and orally efficacious phosphatase inhibitor. *J Med Chem* 2016;**59**:7773–82.
28. Xie J, Si X, Gu S, Wang M, Shen J, Li H, et al. Allosteric inhibitors of SHP2 with therapeutic potential for cancer treatment. *J Med Chem* 2017;**60**:10205–19.
29. Fodor M, Price E, Wang P, Lu H, Argintaru A, Chen Z, et al. Dual allosteric inhibition of SHP2 phosphatase. *ACS Chem Biol* 2018;**13**:647–56.
30. Sarver P, Acker M, Bagdanoff JT, Chen Z, Chen YN, Chan H, et al. 6-Amino-3-methylpyrimidinones as potent, selective, and orally efficacious SHP2 inhibitors. *J Med Chem* 2019;**62**:1793–802.
31. Bagdanoff JT, Chen Z, Acker M, Chen YN, Chan H, Dore M, et al. Optimization of fused bicyclic allosteric SHP2 inhibitors. *J Med Chem* 2019;**62**:1781–92.
32. Wu X, Xu G, Li X, Xu W, Li Q, Liu W, et al. Small molecule inhibitor that stabilizes the autoinhibited conformation of the oncogenic tyrosine phosphatase SHP2. *J Med Chem* 2019;**62**:1125–37.
33. Czako B, Sun Y, McAfoos T, Cross JB, Leonard PG, Burke JP, et al. Discovery of 6-[(3*S*,4*S*)-4-Amino-3-methyl-2-oxa-8-azaspiro[4.5]decan-8-yl]-3-(2,3-dichlorophenyl)-2-methyl-3,4-dihydropyrimidin-4-one (IACS-15414), a potent and orally bioavailable SHP2 inhibitor. *J Med Chem* 2021;**64**:15141–69.
34. Tang K, Wang S, Gao W, Song Y, Yu B. Harnessing the cyclization strategy for new drug discovery. *Acta Pharm Sin B* 2022;**12**:4309–26.
35. LaMarche MJ, Acker M, Argintaru A, Bauer D, Boisclair J, Chan H, et al. Identification of TNO155, an allosteric SHP2 inhibitor for the treatment of cancer. *J Med Chem* 2020;**63**:13578–94.
36. Sun Y, Meyers BA, Czako B, Leonard P, Mseeh F, Harris AL, et al. Allosteric SHP2 Inhibitor, IACS-13909, overcomes EGFR-dependent and EGFR-independent resistance mechanisms toward osimertinib. *Cancer Res* 2020;**80**:4840–53.
37. Taylor AM, Williams BR, Giordanetto F, Kelley EH, Lescarbeau A, Shortsleeves K, et al. Identification of GDC-1971 (RLY-1971), a SHP2 inhibitor designed for the treatment of solid tumors. *J Med Chem* 2023;**66**:13384–99.
38. Drilon A, Sharma MR, Johnson ML, Yap TA, Gadgeel S, Nepert D, et al. SHP2 inhibition sensitizes diverse oncogene-addicted solid tumors to re-treatment with targeted therapy. *Cancer Discov* 2023;**13**:1789–801.
39. Yang X, Xiong J, Yu B, Song Y. Emerging therapeutic approaches of SHP2-targeted modulators. *Future Med Chem* 2024;**16**:291–4.
40. Yang X, Wang Z, Pei Y, Song N, Xu L, Feng B, et al. Discovery of thalidomide-based PROTAC small molecules as the highly efficient SHP2 degraders. *Eur J Med Chem* 2021;**218**:113341.
41. Zheng M, Liu Y, Wu C, Yang K, Wang Q, Zhou Y, et al. Novel PROTACs for degradation of SHP2 protein. *Bioorg Chem* 2021;**110**:104788.
42. Wang M, Lu J, Wang M, Yang CY, Wang S. Discovery of SHP2-D26 as a first, potent, and effective PROTAC degrader of SHP2 protein. *J Med Chem* 2020;**63**:7510–28.
43. Chen X, Shu C, Li W, Hou Q, Luo G, Yang K, et al. Discovery of a novel src homology-2 domain containing protein tyrosine phosphatase-2 (SHP2) and cyclin-dependent kinase 4 (CDK4) dual inhibitor for the treatment of triple-negative breast cancer. *J Med Chem* 2022;**65**:6729–47.
44. Liu M, Gao S, Liang T, Qiu X, Yang X, Fang H, et al. Discovery of novel src homology-2 domain-containing phosphatase 2 and histone deacetylase dual inhibitors with potent antitumor efficacy and enhanced antitumor immunity. *J Med Chem* 2022;**65**:12200–18.
45. Zhang H, Yang X, Song Y, Yu B. Combining EGFR inhibitors with SHP2 or LSD1 inhibitors to overcome multidrug resistance in cancer. *Future Med Chem* 2022;**14**:527–9.

46. Song Y, Zhao M, Wu Y, Yu B, Liu HM. A multifunctional cross-validation high-throughput screening protocol enabling the discovery of new SHP2 inhibitors. *Acta Pharm Sin B* 2021;**11**:750–62.
47. Wang M, Li T, Ouyang Z, Tang K, Zhu Y, Song C, et al. SHP2 allosteric inhibitor TK-453 alleviates psoriasis-like skin inflammation in mice *via* inhibition of IL-23/Th17 axis. *iScience* 2022;**25**:104009.
48. Tang K, Zhao M, Wu YH, Wu Q, Wang S, Dong Y, et al. Structure-based design, synthesis and biological evaluation of aminopyrazines as highly potent, selective, and cellularly active allosteric SHP2 inhibitors. *Eur J Med Chem* 2022;**230**:114106.
49. Copeland RA. *Evaluation of enzyme inhibitors in drug discovery-A guide for medicinal chemists and pharmacologists*. 2nd ed. New Jersey: John Wiley & Sons, Inc.; 2013.